






Article

Magnesium Effect in K/Co-Mg-Mn-Al Mixed Oxide Catalyst for Direct NO Decomposition

Kateřina Karásková ^{1,*}, Kateřina Pacultová ¹ , Anna Klegova ¹, Dagmar Fridrichová ¹, Marta Valášková ¹ , Květuše Jirátová ², Paweł Stelmachowski ³ , Andrzej Kotarba ³  and Lucie Obalová ¹ 

¹ Institute of Environmental Technology, VSB-Technical University of Ostrava, 17. listopadu 15/2172, 70800 Ostrava, Czech Republic; katerina.pacultova@vsb.cz (K.P.); anna.klegova@vsb.cz (A.K.); dagmar.fridrichova@vsb.cz (D.F.); marta.valaskova@vsb.cz (M.V.); lucie.obalova@vsb.cz (L.O.)

² Institute of Chemical Process Fundamentals, Czech Academy of Sciences, Rozvojová 2/135, 16502 Prague, Czech Republic; jiratova@icpf.cas.cz

³ Faculty of Chemistry, Jagiellonian University in Krakow, Gronostajowa 2, PL-30387 Krakow, Poland; pawel.stelmachowski@uj.edu.pl (P.S.); ak@uj.edu.pl (A.K.)

* Correspondence: katerina.karaskova@vsb.cz; Tel.: +420-597-327-329

Received: 9 July 2020; Accepted: 11 August 2020; Published: 13 August 2020



Abstract: Emission of nitric oxide represents a serious environmental problem since it contributes to the formation of acid rain and photochemical smog. Potassium-modified Co-Mn-Al mixed oxide is an effective catalyst for NO decomposition. However, there are problems related to the thermal instability of potassium species and a high content of toxic and expensive cobalt. The reported research aimed to determine whether these shortcomings can be overcome by replacing cobalt with magnesium. Therefore, a series of Co-Mg-Mn-Al mixed oxides with different Co/Mg molar ratio and promoted by various content of potassium was investigated. The catalysts were thoroughly characterized by atomic absorption spectroscopy (AAS), temperature-programmed reduction by hydrogen (TPR-H₂), temperature-programmed desorption of CO₂ (TPD-CO₂), X-ray powder diffraction (XRD), N₂ physisorption, species-resolved thermal alkali desorption (SR-TAD), and tested in direct NO decomposition with and without the addition of oxygen and water vapor. Partial substitution of magnesium for cobalt did not cause an activity decrease when the optimal molar ratio of K/Co on the normalized surface area was maintained; it means that the portion of expensive and toxic cobalt can be successfully replaced by magnesium without any decrease in catalytic activity.

Keywords: cobalt mixed oxide; alkali promoter; nitric oxide; catalytic decomposition

1. Introduction

Nitrogen oxides (NO_x) are not only harmful to the human body but are also responsible for photochemical smog and acid rain. The largest anthropogenic sources of NO_x include exhausts from motor vehicles and fuel combustion. Other sources of NO_x emissions are also chemical processes in which these oxides are present. In the majority of waste gases, more than 95% of NO_x emissions consist of NO. Nitric acid production is an example where NO_x emissions are accompanied by N₂O ones. Direct catalytic decomposition of nitrogen oxides into N₂ and O₂ offers the most ideal route for NO_x removal from waste gases and is both versatile and economic because no reductants (such as NH₃, urea, CO, or hydrocarbons) are required. However, the catalytic activities of catalysts described in literature until now are insufficient, particularly in the presence of other gases such as O₂ and CO₂. For this reason, studies of catalytic decomposition of NO worldwide are still in the stage of basic laboratory

research focused on understanding the mechanisms of catalysts operation in ideal or mild conditions not usable in any real application. However, currently it seems that the most probable application is in stationary combustion processes because the studied catalysts are active at temperatures higher than 600 °C and such high temperatures can be achieved in such processes without additional heating.

Recent progress in catalytic NO decomposition was summarized by Haneda [1], where a historical perspective on catalytic NO decomposition is given. The main piece of knowledge is that for metal oxide catalysts, the overall NO decomposition rate is closely dependent on the rate of O₂ desorption step [2]. Therefore, to develop highly active catalysts for NO decomposition, the creation of catalytically active sites that effectively promote the O₂ desorption step is of critical importance.

In the review [1], many kinds of metal oxides-based catalysts have been reported to catalyze direct NO decomposition. N₂ and O₂ are always formed at steady state with the O₂/N₂ molar ratio of approximately unity and the formation of N₂O is almost negligible in NO decomposition over nonnoble metal oxide-based catalysts. The alkali or alkaline earth metal-doped cobalt oxides represent one group of effective catalysts. In some works [3,4], the presence of residual Na was important to achieve high NO conversion. This interesting effect of residual Na was reported in [5] and later also confirmed by other authors. Haneda et al. [3,4] studied the additive effect of alkali metals on the activity of Co₃O₄ for NO decomposition and they found that the catalytic activity changed with increasing M/Co atomic ratio and the optimal ratio was around 0.02–0.05. The mechanism of alkali and alkaline earth metals promotion has been proposed to be based on structural or electronic effects [6,7]. Since the addition of alkali or alkaline earth metals into Al₂O₃, SiO₂, and ZrO₂ did not increase NO decomposition activity, the interaction between Co₃O₄ and alkali or alkaline earth metal must be an essential factor [4,8]. Potassium deposited on cobalt oxide surface was investigated in [3,9]. It was concluded that the role of potassium was (i) to form the NO₂[−] intermediate and (ii) to keep the cobalt oxide surface partially oxidized so that it can act as an active site for the reaction of the NO₂[−] species. The beneficial effect of potassium addition is strongly related to its location in the catalysts [10].

Calcined layered double hydroxides (LDH, hydrotalcites) are potentially useful as catalysts since they have a high specific surface area and a basic character. In our previous works, the alkali-promoted Co-Mn-Al mixed oxides derived from hydrotalcite precursors were highly active for N₂O decomposition [11–13] and in recent years, similar materials were also proven to be effective catalysts in the NO decomposition reaction [14–16]. However, the long-term activity of these catalysts was compromised by the low stability of alkali metals at reaction temperatures (560–700 °C) caused by their desorption and redistribution. The stabilization of alkali metals can be achieved by adjusting the chemical composition and/or preparation procedure of the catalyst. In [17], the enhancement of potassium stability in the composite ferrite catalyst for ethylbenzene dehydrogenation was achieved by phase-selective doping with Cr, Mn, Ce, Al, and Mg. According to the type of dopant, the additive can increase or decrease potassium stability, thus phase-specific doping appears to be a critical factor in preventing potassium volatilization. In paper [18], it was found that the addition of transition metal elements to the oxide lattice can inhibit the loss of potassium during diesel soot combustion and in [19], it was reported that introduction of alien metal ions, in specific cases, can substantially improve the stability of potassium ferrites. The principal location of potassium remained unchanged by the introduction of the dopants, while the type of stabilization depended on the distribution and placement of the dopants in the catalyst material [20]. Two ways of K desorption prevention were reported: (i) incorporation of the K promoter into the structure, which slows down potassium diffusion from the bulk towards the surface by steric hindrance, and (ii) locating the K promoter at the basal planes, favoring the cationic state of the potassium, which inhibits the probability of potassium atoms leaving the surface via work function increase [19,21].

The catalytic activity of transition metal oxides is closely connected with the valence states of the cations and their coordination in the catalyst matrix. An exemplary study devoted to the elucidation of activities of specific active centers in cobalt spinels for N₂O decomposition was presented by Stelmachowski et al. [22], who assigned the intrinsic activity to octahedral cobalt regardless of the

nature of the cocation. Catalytic performance of the Co-containing metal oxide not only depends on the cobalt content, its oxidation state(s), and location either in octahedral or tetrahedral interstitials but could also be influenced by the Mg/Al ratio [23]. Magnesium and aluminum presence often increases the specific surface area of catalysts [24–26], which plays an important role in the activity of catalysts in many reactions [26,27]. The structural effects of substituting components were also published in [22], where distortion of the spinel structure by the presence of alien cations is reflected in the increase of its reactivity. In addition to that, the cobalt–magnesium interaction was found to be more beneficial to the redox properties of free Co_3O_4 than the cobalt–alumina interaction [28]. Magnesium oxide can also be used as a support for cobalt catalysts, resulting in systems with an improved activity due to the magnesium–cobalt interaction [29,30].

The direct catalytic decomposition of NO proceeds via the following generalized steps [31]: adsorption of NO, reaction of adsorbed NO on the surface leading to the formation of NO_x adspecies, decomposition of NO_x adspecies, desorption of N_2 , and desorption of O_2 . Adsorption of NO has to proceed first to initiate the reaction. As NO molecules can be classified as weak or moderately strong Lewis acids, it would be expected to bind at surface basic sites. The key role of basic sites formed due to the presence of alkali metals in NO adsorption as well as increased storage of NO_x species when alkali or alkali earth metals were introduced to the catalyst surface were confirmed by several authors [32–35].

For this reason, K/Co-Mg-Mn-Al mixed oxides were prepared and applied as catalysts for NO decomposition. The aim of this work was to evaluate the possibility of substituting the cheaper and nature-friendly Mg for the toxic and expensive Co while maintaining the catalyst's activity and simultaneously studying the effect of magnesium on potassium stability. The effects of changing magnesium content while keeping a constant content of potassium and vice versa were studied. The expected advantages of magnesium incorporation were an increase in specific surface area, basicity, and potassium stability.

2. Results

2.1. Characterization of Catalysts

2.1.1. Chemical Composition and Specific Surface Area

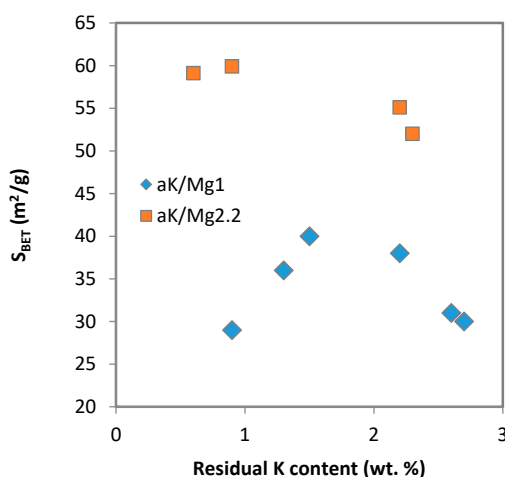
The chemical composition of catalysts calcined at 700 °C was determined by AAS (Table 1). Real (residual) and theoretical (nominal) content of constituent elements were nearly the same. For the 2K/Mg i catalysts (where i denotes the Mg molar content), except for the 2K/Mg2.2 sample (sample with the highest Mg molar content), some small differences in potassium content ranging from 1.4 to 1.8 wt. % of potassium were observed despite having constant nominal K content of 2 wt. %. Potassium content for 2K/Mg2.2 was 2.3 wt. % K. Lower-than-nominal potassium content seems reasonable since potassium vaporization was expected [15,36]. Higher K content (2.3 wt. %) can be caused by a combination of several factors: experimental error during sample preparation and potassium determination and non-homogeneity of samples probably caused by an alkali metal migration process during calcination [36]. No relation between increasing Mg content and residual potassium content was found.

With increasing Mg substitution for Co, an increase of specific surface area occurred. For catalysts containing no potassium, S_{BET} ranged from 36 to 63 $\text{m}^2 \text{g}^{-1}$ (Table 1). A slight decrease in specific surface area caused by potassium modification was observed. Specific surface area was also dependent on K content (Figure 1) and this dependence is evident for the $a\text{K}/\text{Mg}2.2$ series (where a denotes potassium content in wt. %) and especially for the $a\text{K}/\text{Mg}1$ catalysts. An increase in specific surface area was observed with increasing K content up to around 1.5 wt. % of K. When K content became higher than 1.5 wt. %, specific surface area started decreasing.

Table 1. Chemical composition and specific surface area of K/Co-Mg-Mn-Al mixed oxide catalysts.

Sample	Metal Content (wt. %)					Real Molar Ratio	Theoretical Molar Ratio	S_{BET} ($\text{m}^2 \text{g}^{-1}$) ¹	
	K	Co	Mg	Mn	Al	Co:Mg:Mn:Al	Co:Mg:Mn:Al	Fresh	Used
0K/Mg0	0.0	52.1	–	11.7	–	4:0:1:-	4:0:1:1	36	–
0K/Mg0.1	–	–	–	–	–	–	3.9:0.1:1:1	39	–
0K/Mg0.2	–	–	–	–	–	–	3.8:0.2:1:1	41	–
0K/Mg0.5	–	–	–	–	–	–	3.5:0.5:1:1	41	–
0K/Mg1	0.0	42.4	5.3	12.5	6.0	3:0.9:0.9:1	3:1:1:1	44	38
0K/Mg1.6	–	–	–	–	–	–	2.4:1.6:1:1	50	–
0K/Mg2.2	–	–	–	–	–	–	1.8:2.2:1:1	63	–
2K/Mg0	1.9	50.5	0.0	12.0	6.0	4:0:1:1	4:0:1:1	30	–
2K/Mg0.1	1.5	50.8	0.5	11.4	5.5	3.9:0.1:0.9:0.9	3.9:0.1:1:1	38	–
2K/Mg0.2	1.8	50.7	1.1	11.9	6.5	3.8:0.2:1:1.1	3.8:0.2:1:1	37	26
2K/Mg0.5	1.6	45.5	2.5	11.7	6.3	3.5:0.5:1:1.1	3.5:0.5:1:1	41	25
2K/Mg1	1.5	42.0	5.3	12.5	6.7	3:0.9:1:1	3:1:1:1	40	29
2K/Mg1.6	1.4	35.1	8.4	13.1	6.4	2.4:1.4:1:1	2.4:1.6:1:1	44	–
2K/Mg2.2	2.3	27.4	11.9	13.0	6.5	1.8:1.9:0.9:0.9	1.8:2.2:1:1	52	43
1K/Mg1	0.9	42.8	5.2	12.2	6.3	3:0.9:0.9:1	3:1:1:1	29	28
1.5K/Mg1	1.3	42.3	5.2	12.4	6.2	3:0.9:0.9:1	3:1:1:1	36	31
2.5K/Mg1	2.2	41.4	5.2	12.1	6.0	3:0.9:0.9:0.9	3:1:1:1	38	34
3K/Mg1	2.6	41.1	5.1	11.8	6.0	3:0.9:0.9:0.9	3:1:1:1	31	28
4K/Mg1	2.7	39.1	5.1	11.7	6.1	3:0.9:1:1	3:1:1:1	30	27
1K/Mg2.2	0.6	28.4	12.7	13.7	7.2	1.8:2:0.9:1	1.8:2.2:1:1	59	–
1.5K/Mg2.2	0.9	28.0	12.5	13.6	7.3	1.8:1.9:0.9:1	1.8:2.2:1:1	60	–
4K/Mg2.2	2.2	27.7	12.2	13.1	7.0	1.8:1.9:0.9:1	1.8:2.2:1:1	55	–

¹ AutoChem evaluation by the single-point BET equation, $S_{\text{BET}} = (\text{CSA} \cdot 6.023 \times 10^{23}) / (22.414 \times 10^{18} (S + Y))$, where CSA is adsorbate molecular cross-sectional area (0.162 nm^2), S is slope (g/cm^3), and Y is Y-intercept (g/cm^3).

**Figure 1.** Dependence of specific surface area (S_{BET}) on real K content in aK/Mg1 and aK/Mg2.2 catalysts.

A decrease in specific surface area of used catalysts (catalysts after the NO decomposition reaction) in comparison with fresh catalysts was observed (Figure 2). Nevertheless, the trend of specific surface area increase with increasing Mg content was preserved even after the reaction.

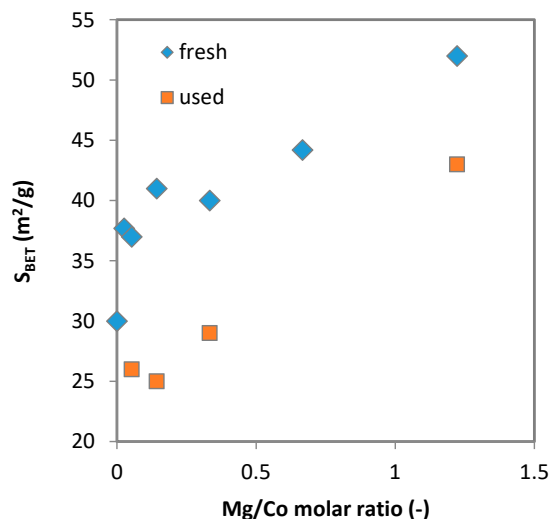


Figure 2. Dependence of S_{BET} on Mg/Co molar ratio for 2K/Mgi catalysts before and after reaction of NO decomposition.

2.1.2. Phase Composition

XRD patterns of catalysts belonging to the 0K/Mgi series are shown in Figure 3. Two different spinel-like phases (S) (Figure 3a) marked as spinel A and B (Figure 3b), Mn_2O_3 (M) (PDF-2 card No. 01-071-0636), and periclase (P) (PDF-2 card No. 01-080-4191) were observed. However, the exact determination of spinel type/composition was impossible because of many possible existing spinel structures having similar structural parameters. For example, in [26], MgCoMnO_4 , MnCo_2O_x , and CoMn_2O_4 were found in XRD patterns of CoMnMgAl mixed oxides calcined at 700 °C, where Mg and Al were substituted with cobalt and manganese. Similarly, the presence of CoAl_2O_4 , Co_2AlO_4 , Co_3O_4 , and MgAl_2O_4 was published in [25]. The 2θ positions of (400) diffraction in the spinel end-members ($\text{Al}_{0.54}\text{Mg}_{0.51}\text{Mn}_{1.95}\text{O}_4$ (PDF No. 01-079-6007), MnCo_2O_4 (PDF No. 00-023-1237), MnAl_2O_4 (PDF No. 00-029-0880), Al_2MgO_4 (PDF No. 01-070-5187), MgCo_2O_4 (PDF No. 01-082-9882), CoAl_2O_4 (PDF No. 00-044-0160), and Co_3O_4 (PDF No. 01-073-1701) were taken from the ICPDF database to provide approximate identification of the type of spinel in the catalyst samples (Figure 4). No strict assignment to specific spinel type was obvious. When the sample contained no magnesium, only spinel A was present. Spinel B occurred just after magnesium substitution and with increasing magnesium content the position of spinel B continually moved to lower 2θ angles indicating an increase of the lattice parameter (Figure 3b and Figure S1a). Contrary to that, the position of (400) reflection of spinel A shifted to higher angles and back (Figure 3b), reflecting different changes of the shape and size of the unit cell. Simultaneously, (400) peak intensity decreased for spinel A and increased for spinel B. Since the XRD peak intensities depend on the position of atoms in the spinel unit cell, it can be assumed that incorporation of Mg into spinel B and redistribution of Co, Mn, and Al took place. Coherent domain size, L_c , decreased for spinel B with increasing Mg/Co molar ratio (Figure S1b) and also with increasing specific surface area (Figure S1c) while similar dependence was not observed for spinel A. The findings also confirm that magnesium, which is responsible for the surface area increase, was mainly incorporated into spinel B. The intensity ratio $I(220/440)$ of diffractions (220) and (440) was found to be sensitive to the cation distribution in the tetrahedral and octahedral sites [37–39] (Figure S2). Continuous decrease of $I(220/440)$ with increasing Mg content in the 0K/Mgi series (Figure S2a) for both spinels (A and B) confirms a gradual rearrangement of the atoms in the spinel unit cell influenced by magnesium substitution. The same trend was also observed for the other two series (2K/Mgi and 4K/Mgi) (Figure S2b,c).

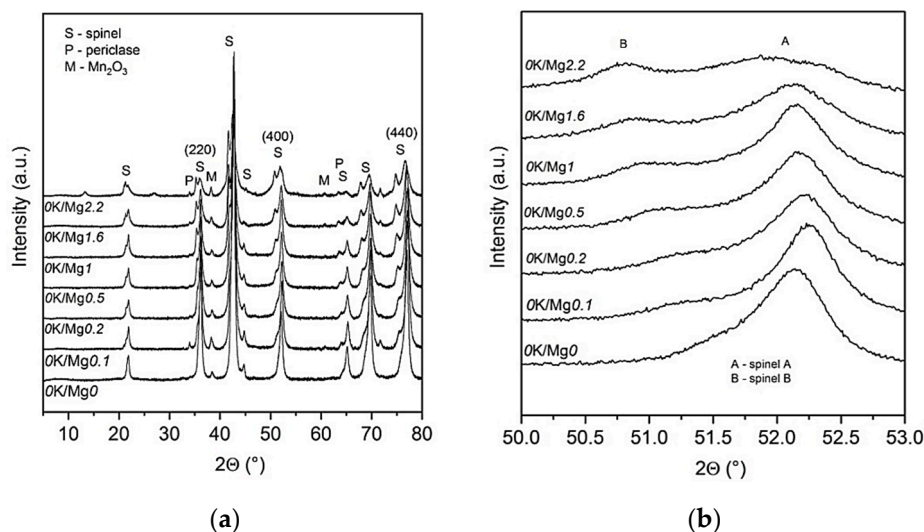


Figure 3. XRD patterns of 0K/Mgi catalysts: (a) from 5° to 80° and (b) from 50° to 53°.

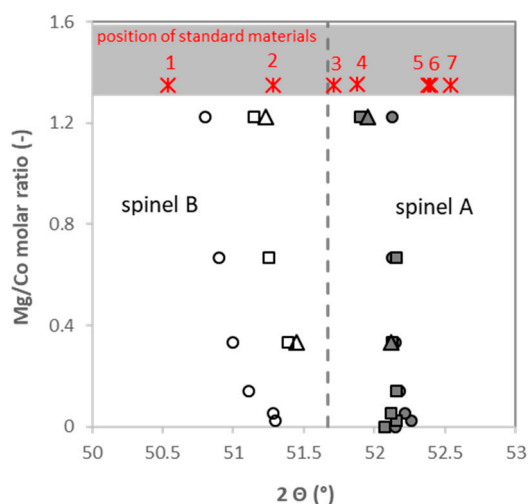


Figure 4. The 2θ positions of (400) diffractions in spinel A and B in the aK/Mg_i catalysts and standard spinel end-members. Legend: circle—0K/Mgi, square—2K/Mgi, triangle—4K/Mgi, 1— $Al_{0.54}Mg_{0.51}Mn_{1.95}O_4$ (PDF No. 01-079-6007), 2— $MnCo_2O_4$ (PDF No. 00-023-1237), 3— $MnAl_2O_4$ (PDF No. 00-029-0880), 4— Al_2MgO_4 (PDF No. 01-070-5187), 5— $MgCo_2O_4$ (PDF No. 01-082-9882), 6— $CoAl_2O_4$ (PDF No. 00-044-0160), and 7— Co_3O_4 (PDF No. 01-073-1701).

For samples containing potassium, the reflections belonging to potassium manganese oxide, attributed to $K_2Mn_4O_8$ (PDF-2, card No. 00-016-0205) and/or $K_{1.39}Mn_3O_6$ (PDF-2, card No. 01-080-7317) were found (Figure 5), which is in accordance with the results reported in [15]. The phases containing potassium and cobalt together were not identified.

The influence of potassium on the XRD patterns of aK/Mg_i catalysts is demonstrated on the 2θ position of diffraction (400) in Figure 4. The position of spinel B shifted to higher diffraction angles after the addition of potassium ranging from 0 to 2 wt. % of K. However, subsequent increase of potassium content above 2 wt. % did not cause any further shift.

The (400) diffraction line position of spinel A was not affected by potassium addition, except for the $aK/Mg_{2.2}$ series, which means that potassium preferentially affected the spinel B structure. Regarding the (220)/(440) intensity ratio sensitivity to the cation distribution, no effect of varying potassium content was observed (Figure S2) for both spinels.

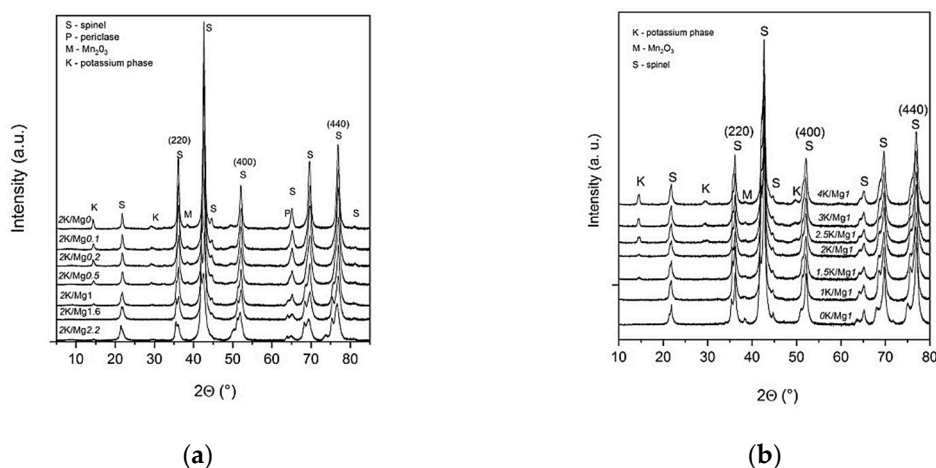


Figure 5. XRD patterns of (a) 2K/Mgi catalysts, (b) and aK/Mg1 catalysts.

2.1.3. TPR-H₂

TPR-H₂ was used to characterize the reducibility of the prepared catalysts (Table 2). Changes in electronic properties combined with structural characteristics of the material can be evaluated from TPR-H₂ and these properties are expected to influence the catalytic activity of investigated samples. The presence of potassium in the samples does not allow performing the TPR-H₂ analysis at high temperatures due to potassium evaporation. For this reason, TPR measurement was performed within the temperature range of 40–600 °C and the subsequent isothermal step at 600 °C for 25 min, giving information about reducible species at a reaction temperature of 600 °C. Hydrogen consumption was calculated for the entire measured temperature region including the isothermal period and ranges from 3.5 to 6.9 mmol H₂ per gram of sample. H₂ consumption decreased with increasing Mg molar content, confirming that reducible cobalt species were replaced by nonreducible magnesium (Figure S3a). The effect of potassium on H₂ consumption was not almost discernible. Only a very gentle increase of reducible species with increasing potassium amount was observed, with the exception of the 4K/Mg1 sample, which possessed a markedly higher amount of species reducible in the low-temperature region (Table 2, Figure S3b).

It is evident from the TPR profiles (Figure S4) that in most cases, the reduction of samples proceeded in two main regions: at 200–500 °C and above 500 °C. In some cases, a change in the trend of the first temperature peak was observed. The reduction of cobalt oxides takes place at similar temperatures as the reduction of manganese oxides [40], which results in overlapping reduction peaks of both compounds in their combined spinels [41]. In the low-temperature region, the reduction of Co³⁺ → Co²⁺ followed by the reduction of Co²⁺ → Co⁰ is accompanied by the reduction of Mn⁴⁺ species and Mn³⁺ to Mn²⁺. The high-temperature peak (>500 °C) was attributed to the reduction of Co ions surrounded by Al ions in a spinel-like phase [12] and the Mn³⁺ to Mn²⁺ reduction, which can take place in both temperature regions. Magnesium oxide is not supposed to be reduced within the studied temperature region [42].

The modification of Co-Mn-Al mixed oxides by magnesium did not cause significant changes in the shapes of TPR-H₂ profiles (Figure S4a). However, for the catalyst with the highest Mg content—0K/Mg2.2, the first peak was lowered by half, which suggests that the 0K/Mg2.2 sample phase composition differs significantly from the rest of the samples, which is in accordance with the XRD findings. From the TPR-H₂ patterns of 2K/Mgi series (Figure S4b), it is evident that the reduction profiles are similar, differing only slightly in low-temperature shoulder progress.

Table 2. Results of temperature-programmed reduction by hydrogen (TPR-H₂) and temperature-programmed desorption of CO₂ (TPD-CO₂) analysis of K/Co-Mg-Mn-Al mixed oxide catalysts.

Sample	TPR-H ₂ (mmol g ⁻¹)	T _{max} (°C) ¹	TPD-CO ₂ (mmol g ⁻¹)	T _{max} (°C) ²
	40–600 °C ¹		28–650 °C	
0K/Mg0	5.8	206, 450	0.2	–
0K/Mg0.1	6.9	435	0.3	–
0K/Mg0.2	–	–	–	–
0K/Mg0.5	5.5	454	0.3	–
0K/Mg1	5.1	461	0.8	–
0K/Mg1.6	–	–	–	–
0K/Mg2.2	3.5	452	1.0	–
2K/Mg0	6.1	317, 398	0.9	404
2K/Mg0.1	6.0	164, 423	0.7	426
2K/Mg0.2	6.0	143, 404	1.2	430
2K/Mg0.5	5.1	437	1.0	422
2K/Mg1	5.1	445	1.9	445
2K/Mg1.6	4.6	433	1.4	416
2K/Mg2.2	4.1	437	2.1	366
1K/Mg1	5.2	145, 449	0.6	370
1.5K/Mg1	5.3	142, 432	0.9	391
2.5K/Mg1	5.4	153, 434	1.5	420
3K/Mg1	5.5	420	1.1	485
4K/Mg1	6.3	169, 303, 390	2.4	363, >600
1K/Mg2.2	4.0	251, 466	0.9	–
1.5K/Mg2.2	4.1	213, 450	1.7	–
4K/Mg2.2	4.2	212, 419	2.2	391

¹ Temperature maximum from TPR-H₂ measurement; ² temperature of the high-temperature peak from TPD-CO₂.

The TPR-H₂ graphical results for the other two groups of catalysts with the same magnesium molar content (Mg = 1 or 2.2 in *a*K/Co_{4-i}Mg_iMnAlO_x) but different potassium content are shown in Figure S4c,d. In both cases, the decrease in the reduction temperature of the low-temperature peak with increasing K content was observed (Figure 6). The same trend—a slight shift of reduction peaks to lower temperatures with increasing K content was also found previously for the Co₄MnAlO_x spinel [12]. In that study, TPR-H₂ was measured up to 1000 °C and a broadening of the high-temperature peak, along with a new peak formation at around 580–620 °C and a new peak (shoulder) formation in the low-temperature region (<300 °C) were observed with increasing K content.

A new reduction peak around 300 °C, sometimes manifesting itself only as a shoulder, was clearly visible in the low-temperature region for the samples with a high content of potassium: 2.5K/Mg1, 3K/Mg1, and 4K/Mg1 (samples from the *a*K/Mg1 catalyst group) (Figure S4c). In the case of the 4K/Mg1 sample, even an additional peak at around 150 °C was observed. The reduction peaks in low temperatures—below 250 °C—may be attributed to the transformation of a CoO₂-like phase to a Co₃O₄-like phase [43]. For catalysts with Mg molar content of 2.2 (the *a*K/Mg2.2 catalyst group), the formation of the low-temperature peak with increasing K content was not observed (Figure S4d); this can be explained by the real (residual) K content in the catalysts, which is lower than in the *a*K/Mg_i series (Table 1). The assignment of the low-temperature shoulder is not fully clear, and different explanations were published in literature [44,45].

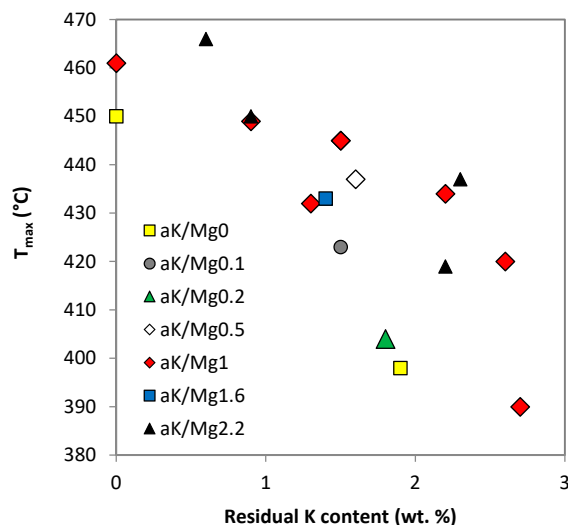


Figure 6. Dependence of T_{\max} of the high-temperature peak from the temperature-programmed reduction by hydrogen (TPR- H_2) measurement on the real K content for K/Co-Mg-Mn-Al mixed oxide catalysts.

2.1.4. TPD- CO_2

The basicity of a deNO catalyst is an important factor influencing chemical reactivity towards NO because of the acidic nature of the NO molecule [14,46] and is also necessary for NO adsorption according to the proposed reaction mechanism pathways [31]. Three major types of basic sites can exist on a metal oxide catalyst surface—weak basic sites represented by OH groups on the catalyst surface, medium basic sites consisting of oxygen in $Me^{2+}-O^{2-}$ and $Me^{3+}-O^{2-}$ pairs, and strong basic sites corresponding to isolated O^{2-} anions [47]. TPD- CO_2 profiles are shown in Figure 7a–d. Similar to the TPR- H_2 measurement, the TPD- CO_2 measurement was also terminated at 650 °C in order to avoid potassium desorption and detector damage.

For samples without potassium (Figure 7a), only one main peak assigned to weak and/or medium basic site was observable. The number and strength of these sites increased with increasing Mg content. Increased number of basic sites, together with their higher strength, was expected after the addition of an alkaline earth component in accordance with published results [48]. Consecutive potassium addition also influenced the number as well as the type of basic sites, as indicated by TPD- CO_2 profile changes (Figure 7b). The number of basic sites for catalysts without potassium is much lower than for K-promoted samples (Table 2, Figure 7a). For K-promoted samples, new desorption peaks above 200 °C, dependent on Mg content, appeared (Figure 7b). The similarities of the types of basic sites defined by T_{\max} at around 350–400 °C were recognized for border cases of 2K/Mg i series—the 2K/Mg0 and 2K/Mg2.2 catalysts. However, these two materials differ in the number of surface basic sites. After careful inspection of the 2K/Mg2.2 catalyst profile, it can be supposed that another maximum at around 460 °C also exists, which was also recognized in the profiles of the rest of the samples of the 2K/Mg i series. The shape of the TPD- CO_2 profiles (Figure 7c,d) was dependent on the K content for all studied catalysts. A second desorption peak appeared from approximately 1.5 wt. % nominal K content and further progress (new high-temperature maxima) was observed with a gradual increase of K content. From the dependence of the number of basic sites on K content, it is evident that CO_2 consumption increased with increasing K content (Figure 8a) regardless of the type of basic sites. The number of specific types of sites (defined by the temperature of desorption) was linearly dependent on the total number of basic sites (Figure 8b). The same trend was observed for the samples without magnesium [12,15].

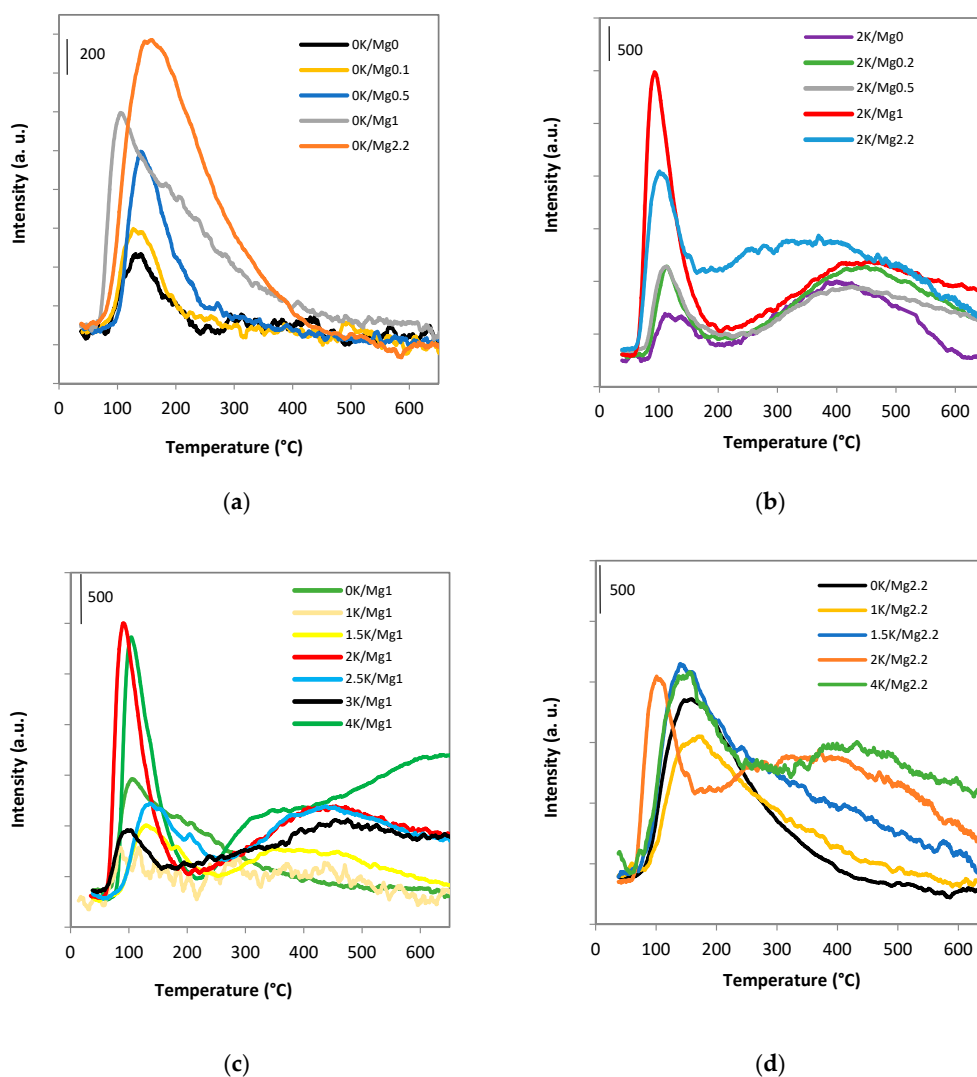


Figure 7. Temperature-programmed desorption of CO_2 (TPD- CO_2) of K/Co-Mg-Mn-Al mixed oxide catalysts: (a) 0K/Mg i catalysts, (b) 2K/Mg i catalysts, (c) a K/Mg1 catalysts, and (d) a K/Mg2.2 catalysts.

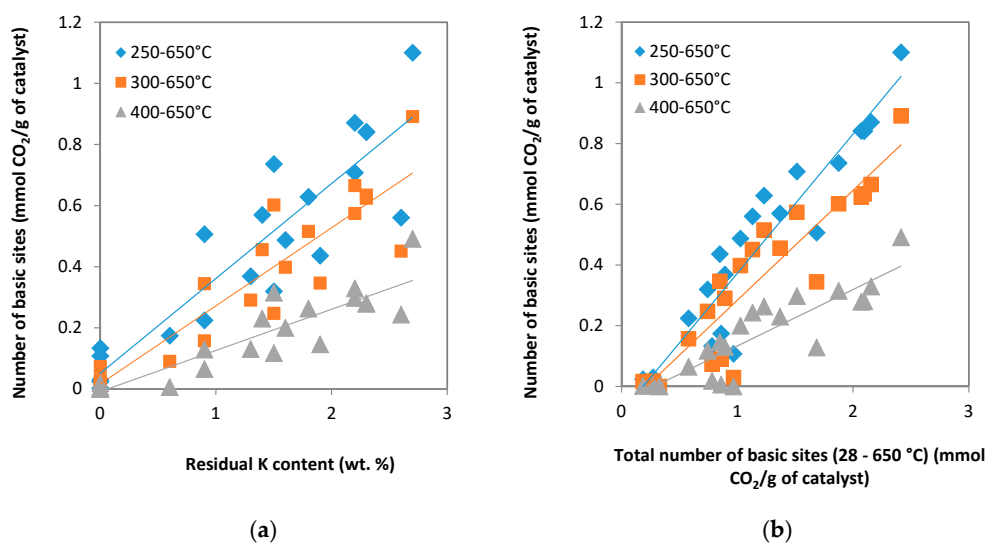


Figure 8. TPD- CO_2 results: (a) dependence of the number of basic sites on the potassium content, and (b) dependence of the number of basic sites (250–650 °C, defined by the temperature region of CO_2 desorption) on the total number of basic sites (28–650 °C).

2.1.5. Species-Resolved Thermal Alkali Desorption

The stability of potassium on the catalyst surface was studied by species-resolved thermal alkali desorption (SR-TAD). Four samples with the same nominal potassium content and different magnesium content (2K/Mgi) were tested. The maximum SR-TAD measurement temperatures are different for each sample since the used experimental set up did not allow fixing the temperature to a constant value. In general, the K–surface bond is broken during the thermal desorption experiment. Thus, the SR-TAD profiles provide information on the surface state of the promoter. Potassium desorption from fresh samples can be observed in vacuum already at temperatures of 400 °C and higher. Monotonic curves of the desorption signal as a function of temperature were observed for all the tested samples (Figure 9). It means that loosely bonded potassium species were already removed from the surface. The exponential components of the signal were always dominant. This indicates that the potassium promoter predominantly leaves the surface through a single energy barrier.

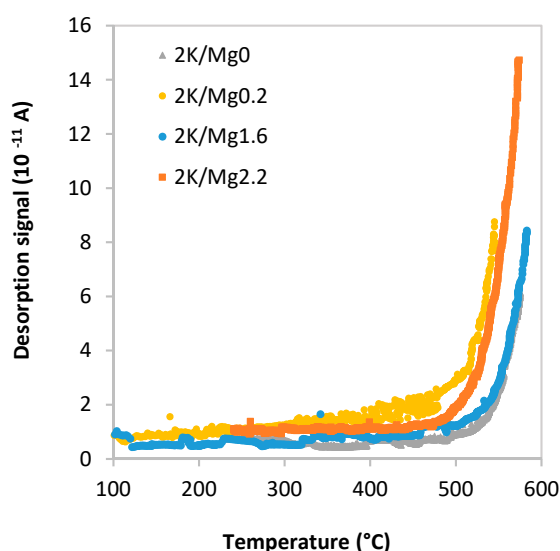


Figure 9. Atomic K desorption flux as a function of temperature.

The intensity of the K atomic desorption flux as a function of the temperature obtained during heating and cooling was almost the same or slightly higher for all samples, with the exception of the 2K/Mg0.2 catalyst (not shown), where substantially higher desorption flux during cooling than during the heating phase was observed. Such changes in the signal suggest that potassium was accumulated and segregated on the surface during the heating. From shapes of the recorded curves, it can be inferred that magnesium content has no direct effect on potassium desorption and, therefore, potassium stabilization on the catalysts' surface.

The desorption activation energies for fresh samples determined from the linear parts of the corresponding Arrhenius-like plots during heating, assuming first-order kinetics, are given in Table 3. The activation energies of desorption correspond to the strength of a surface chemical bond, which breaks during the desorption process and can be used as a suitable parameter for the evaluation of K surface stability [10]. No direct dependence between values of E_a and Mg/Co molar ratio in the catalyst was observed. Although the K desorption results clearly show that potassium became mobile above 500 °C, it has to be remembered that the experiments are performed under high vacuum. The potassium desorption flux will be attenuated by the surrounding gas. Indeed, it was observed that the potassium desorption signals decrease with the pressure as $1/p$ [49].

Table 3. Activation energies of K desorption for selected samples.

Sample	Activation Energy of Potassium Desorption (eV)
2K/Mg0	2.1
2K/Mg0.2	1.4
2K/Mg1.6	1.8
2K/Mg2.2	1.8

2.2. NO Decomposition

The effect of K and Mg content on the catalytic activity of K-promoted Co-Mg-Mn-Al mixed oxides for direct NO decomposition was investigated for NO diluted in an inert atmosphere as well as in the presence of oxygen and water vapor. Apart from catalyst activity and selectivity, characteristics related to stability and the effect of pressure were also evaluated.

2.2.1. Catalytic Activity in Inert Conditions

In our previous work, the effect of calcination temperature, calcination time, potassium content, and the long-term stability of K-promoted Co-Mn-Al mixed oxide in direct NO decomposition was investigated [15]. Stable performance of the catalyst was achieved after 20 h and was maintained for 80 h [15]. For this reason, a stabilization period of at least 20 h was also maintained in this study for all catalysts before measurements of the temperature dependence of NO conversion were performed. As expected from previously reported results [14,15,31], the samples without potassium were inactive at given reaction conditions, and thus, only the results of K-promoted samples are shown. During catalytic tests, the presence of possible reaction products—N₂O and NO₂—was checked, and no formation of N₂O or NO₂ was observed for any sample.

During catalytic measurements, the tested samples showed stable performance and repeated cooling and heating procedures did not influence the obtained NO conversions. The effect of magnesium content on deNO catalyst activity is shown in Figure 10a (for the catalysts with nominal potassium content of 2 wt. %). The sample without Mg was the least active from this group of catalysts; the highest activity was achieved over 2K/Mg1, 2K/Mg0.5, and 2K/Mg0.2 samples (Figure 10a,b).

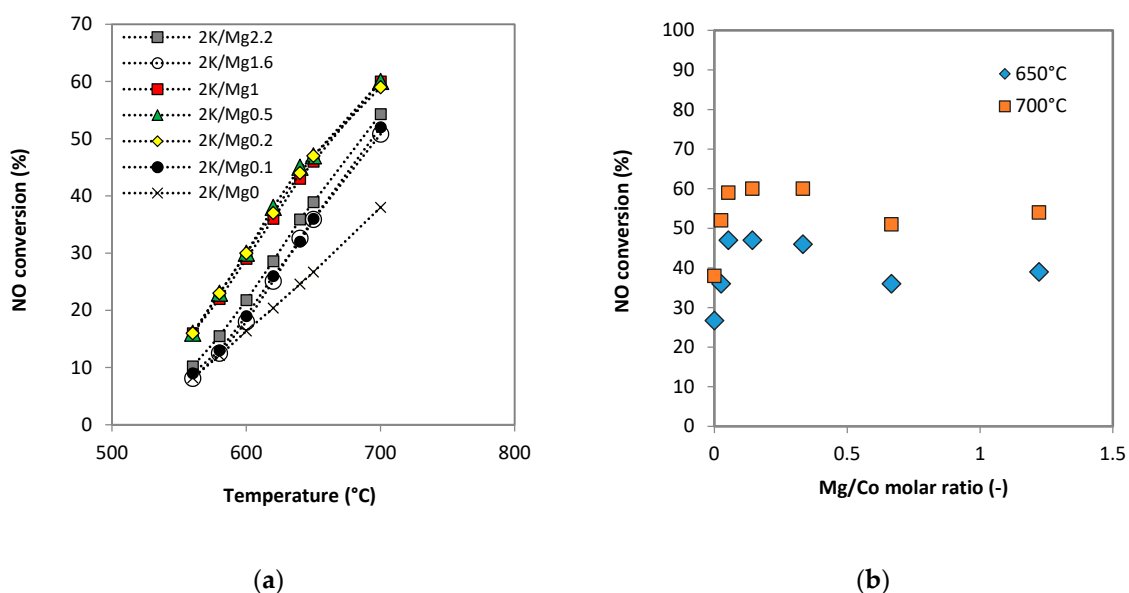


Figure 10. (a) Temperature dependence of NO conversion over the 2K/Mg i group of catalysts and (b) effect of Mg/Co molar ratio on NO conversion over the 2K/Mg i group of catalysts. Conditions: 1000 ppm NO balanced by N₂ and gas hourly space velocity (GHSV) = 6 L g⁻¹ h⁻¹.

The temperature dependence of NO conversion over the *a*K/Mg1 and *a*K/Mg2.2 groups of catalysts, which means catalysts with different wt. % of K (nominal potassium content) and constant content of magnesium, is shown in Figure 11a,b. NO conversion increased with increasing nominal content of potassium up to 2 wt. % (Figure 11a,b); further increase of K content led to a decrease of catalytic activity.

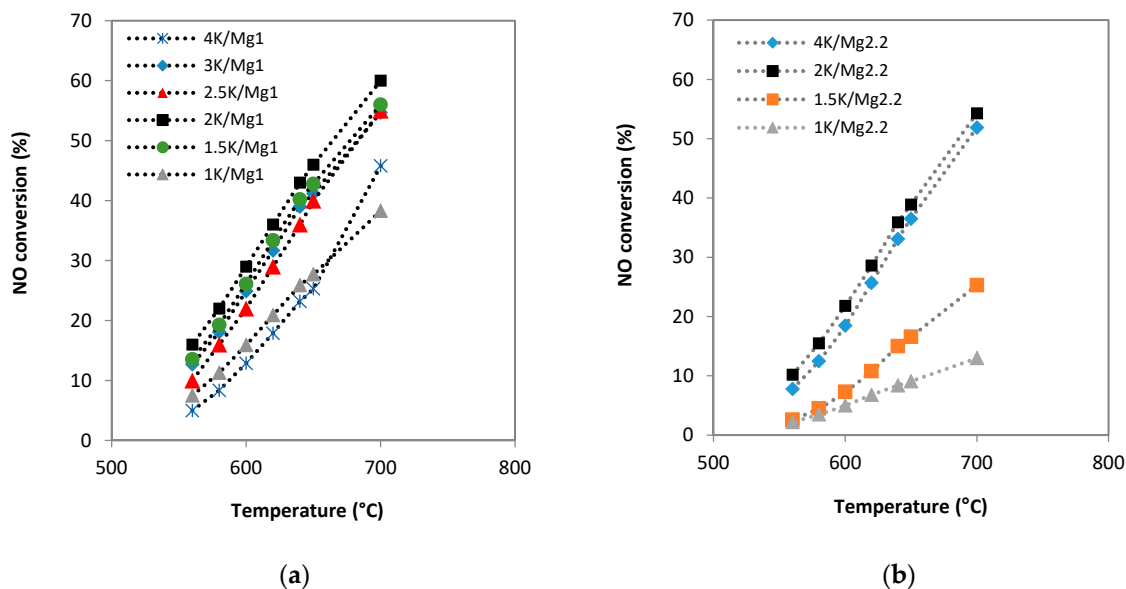


Figure 11. Temperature dependence of NO decomposition over: (a) the *a*K/Mg1 group of catalyst and (b) the *a*K/Mg2.2 group of catalysts. Conditions: 1000 ppm NO balanced by N₂ and GHSV = 6 L g⁻¹ h⁻¹.

2.2.2. Catalytic Activity in the Presence of Oxygen and Water Vapor

The effect of 2 mol. % oxygen in the inlet reaction mixture on direct NO decomposition was also studied (Figure 12a). It is evident that oxygen had a significant inhibitive influence on the activity of all tested samples and the decrease of NO conversion was around 77–90% from the original value in inert gas. Samples that were more active in inert conditions were also more active in the presence of oxygen. Other authors also reported a similar negative effect of oxygen on various types of catalysts [8,31,50,51]. Competitive adsorption of NO and oxygen was suggested based on possible NO decomposition mechanism [31]. After removing oxygen from the inlet gas mixture, the activity of catalysts was restored. This means that the oxygen inhibition effect is reversible (Figure S5).

The effect of H₂O on deNO catalytic activity was tested over the 2K/Mg1 catalyst (Figure 12b). The NO conversion in the gas mixture of 1000 ppm NO + 2 mol. % H₂O balanced by N₂ decreased by half in comparison to inert conditions. It is evident that oxygen had a more significant inhibitive effect on catalytic activity than water vapor. Similar to the effect of oxygen, the effect of water vapor was reversible. Relatively weak inhibition by water in comparison to oxygen was also observed for perovskite type catalysts [52], where it was proposed that hydroxyls on the surface influence the character of the oxygen surface species and, therefore, interfere in the formation of intermediates involving the N–N bond, which is believed to lead to N₂ formation.

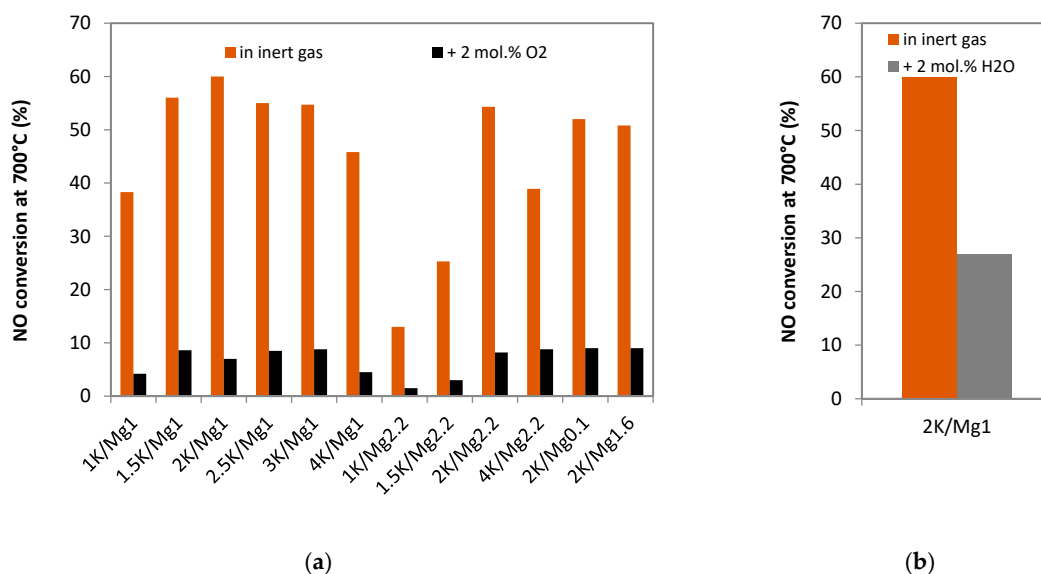


Figure 12. Dependence of NO decomposition over: (a) the aK/Mg_i group of catalysts in inert and oxygen atmosphere and (b) the 2K/Mg1 catalyst in inert and wet atmosphere. Conditions: 1000 ppm NO balanced by N_2 or 1000 ppm NO + 2 mol. % O_2 balanced by N_2 or 1000 ppm NO + 2 mol. % H_2O balanced by N_2 and GHSV = $6 L g^{-1} h^{-1}$.

2.2.3. The Effect of Pressure

For reactions performed in gas phase, it is expected that increasing pressure could increase the rate of reaction. The effect of absolute pressure on NO conversion was tested over 2K/Mg0.2 sample. NO conversion increased with increasing pressure in the reactor (Figure 13). NO conversion increase of about 15% was observed when pressure was increased about 80 kPa. This probative fact shows the necessity to ensure pressure stability during laboratory catalytic experimental testing to guarantee accuracy.

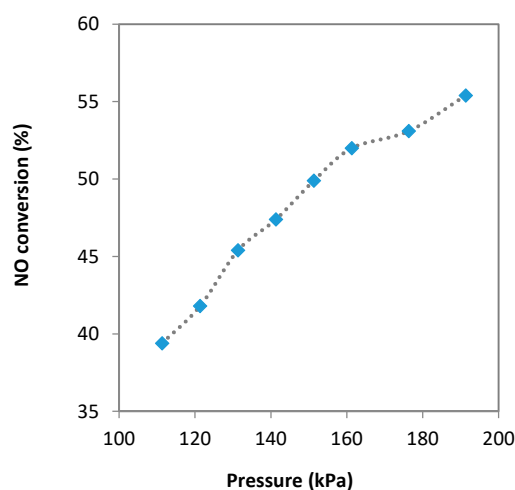


Figure 13. The dependence of NO conversion on pressure over the 2K/Mg0.2 catalyst. Conditions: 1000 ppm NO balanced by N_2 and GHSV = $6 L g^{-1} h^{-1}$.

3. Discussions

Based on the results obtained in this study, physical–chemical properties of the prepared catalysts correlate with their activity for NO decomposition. No dependence of NO conversion on nanocrystal size was observed (not shown). Similarly, dependence of NO activity on specific surface area of the catalyst was not confirmed. Dependence of NO conversion on (i) basic site strength based on the

temperature maxima determined from TPD-CO₂ (Figure 14a), (ii) the number of basic sites (Figure 14b), and (iii) sample reducibility based on the TPR-H₂ low-temperature maximum (Figure 14c) were found. The obtained dependencies are in accordance with the results published in [15], where samples containing no magnesium were tested for NO decomposition. However, in the current work, the determined relations are characterized by an optimal value, while in [15], after achieving the highest values, no distinct maximum or even wide plateau was observed, especially in the case of NO conversion dependence on the number of basic sites. This means that the combination of optimal basicity and reducibility is essential for obtaining high deNO reactivity. Thus, the generation of additional basicity (additional basic sites) via incorporation of other alkaline earth species is pointless in this case. The highest catalytic activity was achieved on catalysts which shared the following characteristics: (i) the main reduction peak is placed at temperatures ranging from 400 to 445 °C, (ii) CO₂ desorption proceeds around 420 °C, and (iii) the number of basic sites determined for the temperature of 300–650 °C ranges from 0.4 to 0.6 mmol CO₂/g. The individual steps of NO decomposition are, in a simplified way: NO adsorption, reaction of adsorbed NO on the surface leading to the formation of surface NO_x species, decomposition of NO_x species, and desorption of N₂ and O₂. Surface basicity is closely related to the NO adsorption and oxidation steps, whereas reducibility is connected with the rate of oxygen desorption from the catalyst surface.

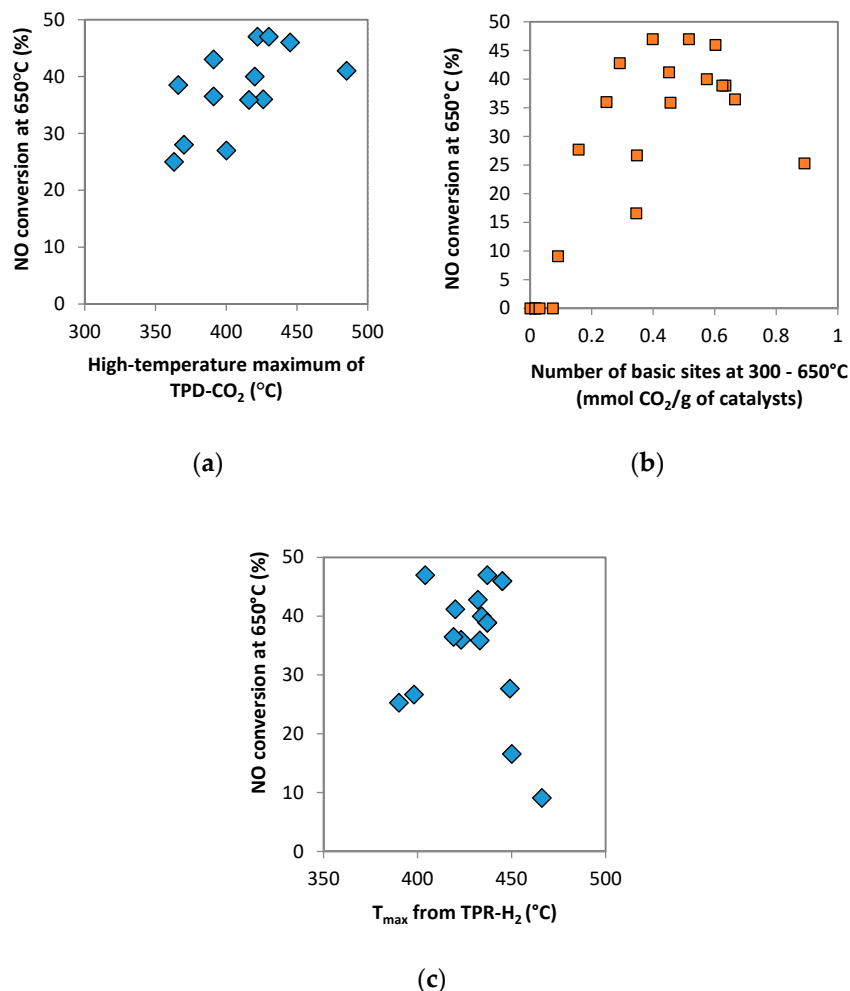


Figure 14. Dependence of NO conversion on: (a) the high-temperature maximum from TPD-CO₂, (b) the number of basic sites, and (c) the temperature maximum from TPR-H₂.

Catalyst reducibility and basicity are dependent on potassium content, as was shown in the characterization part. For this reason, catalytic activity was correlated with the content of potassium

(Figure 15a). Obvious dependence of catalytic activity on K content with a maximum at around 1–2 wt. % of K exists. However, potassium itself is supposed to be inactive and the active sites are formed after the interaction of a transition metal oxide and an alkali metal [3], since alkali metals govern basic properties and influence redox properties, which are derived from transition metals [25]. In our case, it is assumed that Co-K and/or Co-Mn-K can form surface active sites. Although the dependence of NO conversion on Co content was not found (Figure 15b), the dependence of NO conversion on the molar ratio of K/Co (Figure 16a) and K/Mn (not shown) indicate the similar type of dependences—optimal K/Me ratio (Me means transition metal) has to be fixed for optimal catalytic performance. From the obtained results, it is impossible to deduce exactly which transition metal (Co or Mn) represents the active site. In order to explain the individual functions of both metals in NO decomposition, a detailed examination of a series of catalysts with variable content of cobalt and manganese are currently under investigation. In this article, only the effect of cobalt substitution is discussed. An important finding is that the partial substitution of Mg for Co did not cause an activity decrease induced by the decrease of cobalt content in the catalysts if the optimal molar ratio of K/Co was maintained. As much as half of the cobalt in $\text{K/Co}_4\text{MnAlO}_x$ can be replaced by magnesium while keeping high activity. The optimal K/Co ratio was found out to be around 0.05 (Figure 16a), which is in agreement with the results published in [4], where Co_3O_4 promoted by Na, K, Rb, and Cs was studied. The necessity of optimal cobalt and potassium interactions can also be illustrated by the dependence of NO conversion on the normalized cobalt/potassium loading (Figure 16b). It was previously reported [53] that potassium electron donation effect is enhanced with increasing content of potassium. However, when a critical content of potassium is reached for a surface area unit, depolarization effect negatively affects the work function and electronic properties of the catalyst. In our case, the optimal surface concentration of potassium related to the cobalt surface concentration seems to be essential.

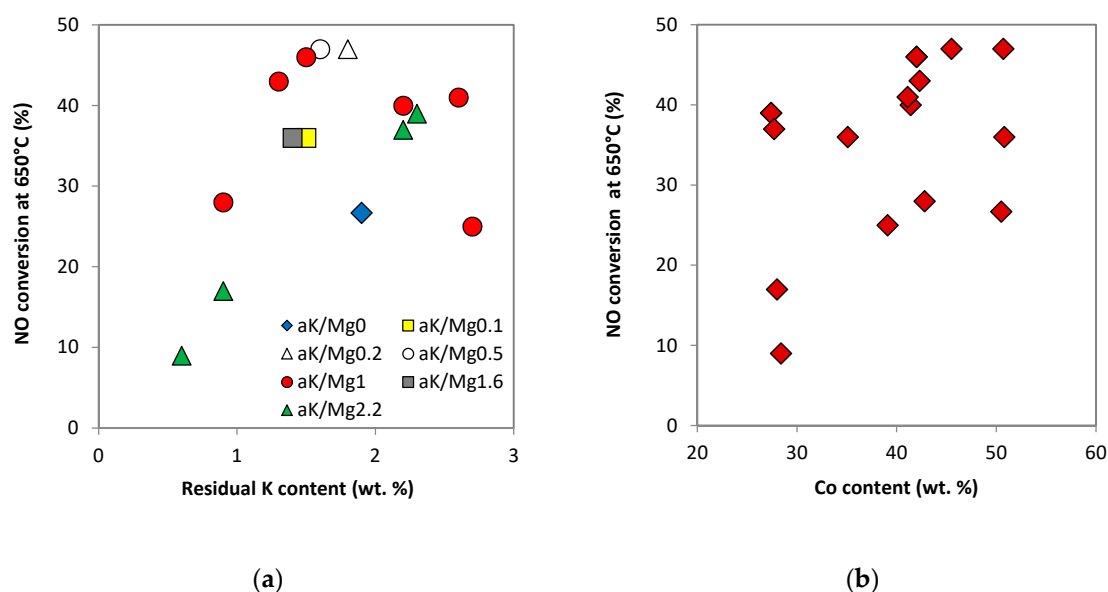


Figure 15. Dependence NO conversion on: (a) residual (real) potassium content and (b) cobalt content.

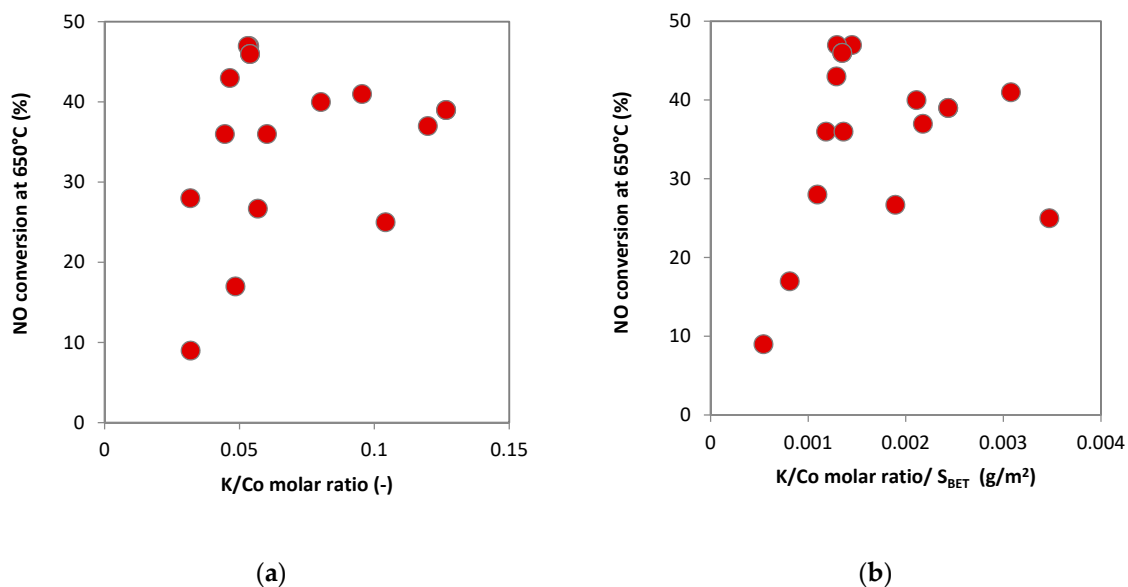


Figure 16. Dependence of NO conversion on: (a) real K/Co molar ratio and (b) K/Co molar ratio to specific surface area.

Potassium desorption activation energies (E_a^{des} , Table 3) correlate with the deNO reactivity of these samples (Figure 10a). A monotonous increase of NO conversion for a given reaction temperature is observed with the decrease of the E_a^{des} (Figure S6). Thus, the K-surface interaction strength plays a crucial role in governing catalytic activity. The potassium surface state is also reflected in the basicity and reducibility of the samples.

Regardless of the optimal K/Co ratio, it is clear that if partial magnesium substitution did not cause a decrease in catalyst activity, only a part of initially present cobalt species was directly responsible for NO decomposition. It is known that transition metal ion coordination exerts a huge influence on its catalytic activity in various reactions [22,26]. In mixed oxides with spinel structure, elements are distributed in both octahedral and tetrahedral sites. Concerning applications in catalysis, the catalytic activity of spinels depends essentially on the degree of tetrahedral sites substitution and the degree of inversion of the spinel [54]. From octahedral site preference energies of ions, we can assume that Co^{3+} , Mn^{4+} , Mn^{3+} , and Al^{3+} ions are predominantly placed in octahedral sites, whereas Mn^{2+} , Co^{2+} , and Mg^{2+} ions preferentially occupy tetrahedral sites when incorporated in the spinel matrix. Mg^{2+} should thus substitute Co^{2+} in tetrahedral positions after cobalt substitution. Similar to the results of Stelmachowski et al. [22], who studied N_2O decomposition, the octahedral cobalt species seems to also be important for NO decomposition.

4. Materials and Methods

4.1. Catalyst Preparation

The Co-Mg-Mn-Al LDH precursors with (Co + Mg):Mn:Al molar ratio of 4:1:1 were prepared by coprecipitation of the corresponding nitrates ($\text{Co}(\text{NO}_3)_2 \cdot 6 \text{H}_2\text{O}$, $\text{Mn}(\text{NO}_3)_2 \cdot 4 \text{H}_2\text{O}$, $\text{Al}(\text{NO}_3)_3 \cdot 9 \text{H}_2\text{O}$, and $\text{Mg}(\text{NO}_3)_2 \cdot 6 \text{H}_2\text{O}$) in $\text{Na}_2\text{CO}_3/\text{NaOH}$ solution at 30 °C and pH 10. The washed and dried products were calcined for 4 h at 670 or 700 °C in air. The prepared mixed oxides were crushed and sieved to obtain a fraction with a particle size of 0.016–0.315 mm. Samples calcined at 700 °C were directly used for catalytic measurements. These catalysts were examined as reference samples.

Further, potassium was used as a promoter for modification of the prepared Co-Mg-Mn-Al mixed oxides calcined at 670 °C. The modification was done by impregnation with KNO_3 solution by the pore-filling method. KNO_3 solution with different concentrations was added to Co-Mg-Mn-Al mixed oxide to achieve the desired (nominal) K content; the mixture was matured for 1 h. After drying at

105 °C for 4 h, the impregnated samples were calcined at 700 °C for 4 h and sieved to 0.016–0.315 mm fraction. The samples were labeled according to their nominal (intended) potassium and magnesium content, e.g., 2K/Mg0.2 means that the Co:Mg:Mn:Al molar ratio in the samples is 3.8:0.2:1:1 and the mixed oxide catalyst was modified by 2 wt. % of potassium. The list of prepared samples is given in Table 1. When referencing the series with a constant Mg content and different K content or vice versa, abbreviations using the symbols *a* or *i* are used, e.g., *a*K/Mg*i*, and these denote the K wt. % or Mg molar content in Co_{4-i}Mg_iMnAlO_x, respectively. The *x* denotes molar fraction of oxygen, which is unknown but theoretically should approach 8.

4.2. Catalyst Characterization

Chemical composition of the prepared catalysts was determined by atomic absorption spectroscopy (AAS) using the Analytik Jena ContraAA 700 spectrometer after dissolving approximately 50 mg of the sample (powder form) in aqua regia acid by heating it to 200 °C in the Ethos UP microwave reactor (Milestone Ethos Up, Sorisole, Italy). Details are given in [15].

Phase composition was determined using the X-ray powder diffraction (XRD) technique. The XRD patterns were recorded under CoK α radiation ($\lambda_1 = 0.1789$ nm and $\lambda_2 = 0.1793$ nm) using the Rigaku SmartLab diffractometer (Rigaku Corporation, Tokyo, Japan) equipped with the D/teX Ultra 250 detector (Rigaku Corporation, Tokyo, Japan). Further details are published in [15]. Measurements were carried out in reflection mode; powdered samples were pressed in a rotational holder; a goniometer with the Bragg-Brentano geometry in 2θ range from 5° to 90°, step size 0.01°, was used. The phase composition was evaluated using the PDF-2 (International Centre for Diffraction Data) database.

Temperature-programmed reduction by hydrogen (TPR-H₂) was carried out on the AutoChem II-2920 system (Micromeritics, Atlanta, GA, USA). Before each TPR-H₂ experiment, the sample (0.08 g, 0.160–0.315 mm) was pretreated in Ar (50 mL min⁻¹) at 600 °C for 1 h. After cooling to 40 °C in the same atmosphere, a hydrogen–argon mixture (10 mol. % H₂/Ar) was used to reduce the sample at a flow of 50 mL min⁻¹. The temperature was linearly increased at a rate of 20 °C min⁻¹ up to 600 °C. After reaching 600 °C, the temperature was kept constant for 20 min. Water vapor formed during the TPR measurements was captured in a cold trap.

Temperature-programmed desorption of CO₂ (TPD-CO₂) was carried out on the AutoChem II-2920 system (Micromeritics, Atlanta, GA, USA) connected on-line to a mass spectrometer (Prevac, Rogów, Poland). Prior to CO₂ adsorption, the catalysts (0.08 g, 0.160–0.315 mm) were heated up to 650 °C in He for 1 h (flow rate of 50 mL min⁻¹). Then, the sample was cooled and the adsorption of CO₂ (50 mol. % CO₂ in He) was performed at 28 °C for 1 h. To remove physically adsorbed CO₂, the samples were purified for 105 min in helium stream (50 mL/min) at 28 °C. TPD-CO₂ was carried out on catalysts using helium as a carrier gas (50 mL min⁻¹). The desorption of CO₂ was induced by heating (20 °C min⁻¹) up to a final temperature of 650 °C. The temperature was kept constant for 10 min.

N₂ physisorption at 196 °C was performed on the AutoChem II-2920 system (Micromeritics, Atlanta, GA, USA), and the single-point BET method was used for specific surface area evaluation. Before analysis, each sample was degassed for 1 h at 450 °C in He flow of 50 mL min⁻¹. After degassing, a mixture of 30 mol. % N₂ and 70 mol. % He was applied to the sample that was immersed in liquid nitrogen. The amount of N₂ adsorbed at liquid nitrogen temperature was used to calculate the surface area.

Thermal stability of the potassium promoter was investigated by the species-resolved thermal alkali desorption (SR-TAD) method. The experiments were carried out in a vacuum apparatus with a background pressure of 10⁻⁷ kPa. The samples in the form of wafers (13 mm diameter and 100 mg weight) were heated up from room temperature to 560 °C in stepwise mode by increasing the electric current flowing through the heater plate. The desorption flux of potassium atoms was determined by means of a surface ionization detector. During the measurements, the samples were biased with a positive potential (+10 V) to quench the thermal emission of electrons. In all measurements, the

resulting positive current was directly measured with the Keithley 6512 digital electrometer (Keithley, Cleveland, OH, USA).

4.3. Catalytic Measurement

Catalytic decomposition of NO was performed in a tubular stainless-steel reactor with 6 mm internal diameter in the temperature range of 560–700 °C under atmospheric pressure. When the effect of pressure was tested, the pressure of 111.325–191.325 kPa was applied. The gradual increase of pressure was set by a needle valve located downstream of the reactor and upstream of the IR analyzer. The total flow rate was 49 mL min⁻¹ (NTP). The catalyst bed contained 0.5 g of the catalyst with particle size of 0.160–0.315 mm leading to gas hourly space velocity (GHSV) of 5.88 L g_{cat}⁻¹ h⁻¹. The inlet gas contained 0.1 mol. % NO in nitrogen, while 2 mol. % O₂ or 2 mol. % H₂O was introduced to some runs. A temperature-controlled furnace heated the reactor.

Before the first catalytic run, the catalyst was pretreated in an oxygen (20 mol. %)/N₂ mixture at 650 °C for 1 h. Then the reaction was started and NO catalytic decomposition at 650 °C was measured for 24 h at least. After this period, when stable performance was observed, the test of conversion dependence on temperature was launched with a cooling rate of 5 °C min⁻¹ and the catalyst activity was measured for 3 h at each temperature (640, 620, 600, 580, and 560 °C). Then the stability of catalysts at 650 °C was tested (Figure S7). In case the performance was stable, the catalyst was heated to 700 °C. Finally, NO decomposition in inert gas and in the presence of 2 mol. % oxygen or in the presence of 2 mol. % water vapor at 700 °C was measured. NO concentration achieved at steady state was used for calculation of NO conversion.

The ULTRAMAT 6 infrared analyzer (Siemens, Karlsruhe, Germany) was used for online analysis of NO. The low-temperature NO₂/NO converter (TESO Ltd., Prague, Czech Republic) was connected to the NO analyzer in bypass mode and was periodically switched to conversion mode in order to analyze the sum of NO_x and thus control the amount of NO₂. The presence of N₂O was controlled on FTIR spectrometer (Antaris IGS) (Nicolet, Prague, Czech Republic). The error of NO conversion was determined by repeated measurements as ±5% (absolute error).

5. Conclusions

From the results obtained in this work, we can conclude that K/Co-Mg-Mn-Al mixed oxides promoted by potassium are active in direct NO decomposition. However, the presence of oxygen negatively influenced their catalytic activity. Water vapor inhibition showed a much less significant effect on catalytic activity than oxygen. The formation of a potassium-manganese oxide phase was observed with increasing K content in the catalysts with constant Mg content. The presence of potassium increased catalysts' basicity and improved reducibility. Both factors are necessary for the activation of the NO molecule and oxygen desorption and both influenced the catalytic deNO activity. Substitution of magnesium for cobalt in the spinel structure led to increased specific surface area but no correlation between specific surface area and NO conversion was observed. Although there was no direct correlation of K stability with Mg content, a direct correlation between the activation energy of potassium desorption and deNO catalytic activity was found. Partial substitution of magnesium for cobalt did not decrease the activity if the optimal molar ratio of K/Co on the unit surface area was maintained. It means that as much as half of the potentially toxic and expensive cobalt species can be easily replaced with magnesium without any activity loss.

Supplementary Materials: The following are available online at <http://www.mdpi.com/2073-4344/10/8/931/s1>, Figure S1: Dependence of (a) lattice parameter *a* on Mg/Co molar ratio, (b) coherent domain size *L_c* on Mg/Co molar ratio, and (c) coherent domain size *L_c* on specific surface area for spinel B; Figure S2: Intensity ratio *I* (220)/(440) for (a) 0K/Mgi, (b) 2K/Mgi, and (c) 4K/Mgi; Figure S3: Consumed amount of H₂ during TPR-H₂ for: (a) 0K/Mgi and 2K/Mgi catalysts and (b) aK/Mg1 and aK/Mg2.2 catalysts; Figure S4: TPR-H₂ of K/Co-Mg-Mn-Al mixed oxide catalysts: (a) 0K/Mgi catalysts, (b) 2K/Mgi catalysts, (c) aK/Mg1 catalysts, and (d) aK/Mg2.2 catalysts. Figure S5: Time on stream dependence of NO conversion; Figure S6: Dependence of NO conversion on potassium desorption activation energies; Figure S7: Catalytic measurement procedure-stability verification.

Author Contributions: Conceptualization, K.K. and K.P.; data curation, K.K., K.P., D.F., M.V., and P.S.; investigation, K.K., K.P., A.K. (Anna Klegova), D.F., and P.S.; methodology, K.K., K.P., and A.K. (Andrzej Kotarba); project administration, K.P., K.J., and L.O.; supervision, L.O.; writing—original draft, K.K.; writing—review and editing, K.P., M.V., K.J., P.S., A.K. (Andrzej Kotarba), and L.O. All authors have read and approved the final version of the manuscript.

Funding: This research was funded by ERDF “Institute of Environmental Technology—Excellent Research” (No. CZ.02.1.01/0.0/0.0/16_019/0000853 and by Czech Science Foundation (project No. 18-19519S.). Experimental results were accomplished by using Large Research Infrastructures ENREGAT (No. LM2018098) and CATPRO (LM2015039) supported by the Ministry of Education, Youth and Sports of the Czech Republic.

Acknowledgments: We thank Zdeněk Tišler from UniCRE, Unipetrol Centre for Research and Education, a.s. for precursor preparation and Alexandr Martaus from Institute of Environmental Technology, VSB–Technical University of Ostrava for the XRD measurements.

Conflicts of Interest: The authors declare no conflict of interest. The funders had no role in the design of the study; in the collection, analyses, or interpretation of data; in the writing of the manuscript; or in the decision to publish the results.

References

1. Haneda, M.; Hamada, H. Recent progress in catalytic NO decomposition. *Comptes Rendus Chim.* **2016**, *19*, 1254–1265. [[CrossRef](#)]
2. Winter, E.R.S. The catalytic decomposition of nitric oxide by metallic oxides. *J. Catal.* **1971**, *22*, 158–170. [[CrossRef](#)]
3. Haneda, M.; Kintaichi, Y.; Bion, N.; Hamada, H. Alkali metal-doped cobalt oxide catalysts for NO decomposition. *Appl. Catal. B: Environ.* **2003**, *46*, 473–482. [[CrossRef](#)]
4. Haneda, M.; Nakamura, I.; Fujitani, T.; Hamada, H. Catalytic Active Site for NO Decomposition Elucidated by Surface Science and Real Catalyst. *Catal. Surv. Asia* **2005**, *9*, 207–215. [[CrossRef](#)]
5. Park, P.W.; Kil, J.K.; Kung, H.H.; Kung, M.C. NO decomposition over sodium-promoted cobalt oxide. *Catal. Today* **1998**, *42*, 51–60. [[CrossRef](#)]
6. Konsolakis, M.; Yentekakis, I.V. The reduction of NO by propene over Ba-promoted Pt/gamma-Al₂O₃ catalysts. *J. Catal.* **2001**, *198*, 142–150. [[CrossRef](#)]
7. Konsolakis, M.; Yentekakis, I.V. Strong promotional effects of Li, K, Rb and Cs on the Pt-catalysed reduction of NO by propene. *Appl. Catal. B: Environ.* **2001**, *29*, 103–113. [[CrossRef](#)]
8. Iwamoto, S.; Takahashi, R.; Inoue, M. Direct decomposition of nitric oxide over Ba catalysts supported on CeO₂-based mixed oxides. *Appl. Catal. B: Environ.* **2007**, *70*, 146–150. [[CrossRef](#)]
9. Nakamura, I.; Haneda, M.; Hamada, H.; Fujitani, T. Direct decomposition of nitrogen monoxide over a K-deposited Co (0001) surface: Comparison to K-doped cobalt oxide catalysts. *J. Electron. Spectrosc. Relat. Phenom.* **2006**, *150*, 150–154. [[CrossRef](#)]
10. Borowiecki, T.; Denis, A.; Rawski, M.; Gołębiowski, A.; Stołeczki, K.; Dmytryk, J.; Kotarba, A. Studies of potassium-promoted nickel catalysts for methane steam reforming: Effect of surface potassium location. *Appl. Surf. Sci.* **2014**, *300*, 191–200. [[CrossRef](#)]
11. Karásková, K.; Obalová, L.; Kovanda, F. N₂O catalytic decomposition and temperature programmed desorption tests on alkali metals promoted Co-Mn-Al mixed oxide. *Catal. Today* **2011**, *176*, 208–211. [[CrossRef](#)]
12. Obalová, L.; Karásková, K.; Jiráťová, K.; Kovanda, F. Effect of potassium in calcined Co-Mn-Al layered double hydroxide on the catalytic decomposition of N₂O. *Appl. Catal. B: Environ.* **2009**, *90*, 132–140. [[CrossRef](#)]
13. Obalová, L.; Karásková, K.; Wach, A.; Kustrowski, P.; Mamulová-Kutlákova, K.; Michalik, S.; Jiráťová, K. Alkali metals as promoters in Co-Mn-Al mixed oxide for N₂O decomposition. *Appl. Catal. A-Gen.* **2013**, *462*, 227–235. [[CrossRef](#)]
14. Pacultová, K.; Draštková, V.; Chromčáková, Ž.; Bílková, T.; Kutlákova, K.M.; Kotarba, A.; Obalová, L. On the stability of alkali metal promoters in Co mixed oxides during direct NO catalytic decomposition. *Mol. Catal.* **2017**, *428*, 33–40. [[CrossRef](#)]
15. Pacultová, K.; Bílková, T.; Klegova, A.; Karásková, K.; Fridrichová, D.; Jiráťová, K.; Kiška, T.; Balabánová, J.; Koštejn, M.; Kotarba, A.; et al. Co-Mn-Al Mixed Oxides Promoted by K for Direct NO Decomposition: Effect of Preparation Parameters. *Catalysts* **2019**, *9*, 593. [[CrossRef](#)]

16. Jiráťová, K.; Pacultová, K.; Balabánová, J.; Karásková, K.; Klegova, A.; Bílková, T.; Jandová, V.; Koštejn, M.; Martaus, A.; Kotarba, A.; et al. Precipitated K-Promoted Co-Mn-Al Mixed Oxides for Direct NO Decomposition: Preparation and Properties. *Catalysts* **2019**, *9*, 592. [[CrossRef](#)]
17. Kotarba, A.; Rožek, W.; Serafin, I.; Sojka, Z. Reverse effect of doping on stability of principal components of styrene catalyst: KFeO_2 and $\text{K}_2\text{Fe}_{22}\text{O}_{34}$. *J. Catal.* **2007**, *247*, 238–244. [[CrossRef](#)]
18. An, H.; McGinn, P.J. Catalytic behavior of potassium containing compounds for diesel soot combustion. *Appl. Catal. B: Environ.* **2006**, *62*, 46–56. [[CrossRef](#)]
19. Bieniasz, W.; Trębala, M.; Sojka, Z.; Kotarba, A. Irreversible deactivation of styrene catalyst due to potassium loss—Development of antidote via mechanism pinning. *Catal. Today* **2010**, *154*, 224–228. [[CrossRef](#)]
20. Trębala, M.; Bieniasz, W.; Holmlid, L.; Molenda, M.; Kotarba, A. Potassium stabilization in $\beta\text{-K}_2\text{Fe}_{22}\text{O}_{34}$ by Cr and Ce doping studied by field reversal method. *Solid State Ion.* **2011**, *192*, 664–667. [[CrossRef](#)]
21. Kotarba, A.; Bieniasz, W.; Kuśtrowski, P.; Stadnicka, K.; Sojka, Z. Composite ferrite catalyst for ethylbenzene dehydrogenation: Enhancement of potassium stability and catalytic performance by phase selective doping. *Appl. Catal. A: Gen.* **2011**, *407*, 100–105. [[CrossRef](#)]
22. Stelmachowski, P.; Maniak, G.; Kaczmarczyk, J.; Zasada, F.; Piskorz, W.; Kotarba, A.; Sojka, Z. Mg and Al substituted cobalt spinels as catalysts for low temperature deN_2O —Evidence for octahedral cobalt active sites. *Appl. Catal. A: Gen.* **2014**, *146*, 105–111. [[CrossRef](#)]
23. Basag, S.; Kovanda, F.; Piwowska, Z.; Kowalczyk, A.; Pamin, K.; Chmielarz, L. Hydrotalcite-derived Co-containing mixed metal oxide catalysts for methanol incineration Role of cobalt content, Mg/Al ratio and calcination temperature. *J. Therm. Anal. Calorim.* **2017**, *129*, 1301–1311. [[CrossRef](#)]
24. Tao, Y.X.; Yu, J.J.; Liu, C.C.; Hao, Z.P. N_2O catalytic decomposition over mixed oxides derived from Co-Mg/Al hydrotalcite-like compounds. *Acta Phys.-Chim. Sin.* **2007**, *23*, 162–168.
25. Palomares, E.; Uzcátegui, A.; Franch, C.; Corma, A. Multifunctional catalyst for maximizing NO_x oxidation/storage/reduction: The role of the different active sites. *Appl. Catal. B: Environ.* **2013**, *142*, 795–800. [[CrossRef](#)]
26. Mokhtar, M.; Basahel, S.N.; Al-Angary, Y.O. Nanosized spinel oxide catalysts for CO-oxidation prepared via CoMnMgAl quaternary hydrotalcite route. *J. Alloys Compd.* **2010**, *493*, 376–384. [[CrossRef](#)]
27. Castaño, M.H.; Molina, R.; Moreno, S. Mn–Co–Al–Mg mixed oxides by auto-combustion method and their use as catalysts in the total oxidation of toluene. *J. Mol. Catal. A: Chem.* **2013**, *370*, 167–174. [[CrossRef](#)]
28. Choya, A.; de Rivas, B.; González-Velasco, J.R.; Gutiérrez-Ortiz, J.I.; López-Fonseca, R. On the beneficial effect of MgO promoter on the performance of $\text{Co}_3\text{O}_4/\text{Al}_2\text{O}_3$ catalysts for combustion of dilute methane. *Appl. Catal. A-Gen.* **2019**, *582*, 117099. [[CrossRef](#)]
29. Ulla, M.A.; Spretz, R.; Lombardo, E.; Daniell, W.; Knozinger, H. Catalytic combustion of methane on Co/MgO: Characterisation of active cobalt sites. *Appl. Catal. B: Environ.* **2001**, *29*, 217–229. [[CrossRef](#)]
30. Ji, S.F.; Xiao, T.C.; Wang, H.T.; Flahaut, E.; Coleman, K.S.; Green, M.L.H. Catalytic combustion of methane over cobalt-magnesium oxide solid solution catalysts. *Catal. Lett.* **2001**, *75*, 65–71. [[CrossRef](#)]
31. Haneda, M.; Kintaichi, Y.; Hamada, H. Reaction mechanism of NO decomposition over alkali metal-doped cobalt oxide catalysts. *Appl. Catal. B: Environ.* **2005**, *55*, 169–175. [[CrossRef](#)]
32. Bai, Z.; Chen, B.; Zhao, Q.; Shi, C.; Crocker, M. Positive effects of K^+ in hybrid CoMn-K and Pd/Ba/ Al_2O_3 catalysts for NO_x storage and reduction. *Appl. Catal. B* **2019**, *249*, 333–345. [[CrossRef](#)]
33. Li, Q.; Meng, M.; Tsubaki, N.; Li, X.; Li, Z.; Xie, Y.; Hu, T.; Zhang, J. Performance of K-promoted hydrotalcite-derived CoMgAlO catalysts used for soot combustion, NO_x storage and simultaneous soot- NO_x removal. *Appl. Catal. B* **2009**, *91*, 406–415. [[CrossRef](#)]
34. Le-Phuc, N. Removal of NO_x in the presence of oxygen over Mn/BaO/ Al_2O_3 catalysts. *Mater. Sci. Nanotechnol.* **2017**, *2*, 37–40. [[CrossRef](#)]
35. Chen, H.; Zhang, Y.; Xin, Y.; Li, Q.; Zhang, Z.; Jiang, Z.; Ma, Y.; Zhou, H.; Zhang, J. Enhanced NO_x conversion by coupling NO_x storage-reduction with CO adsorption-oxidation over the combined Pd–K/MgAlO and Pd/MgAlO catalysts. *Catal. Today* **2015**, *258*, 416–423. [[CrossRef](#)]
36. Grzybek, G.; Wójcik, S.; Legutko, P.; Gryboś, J.; Indyka, P.; Leszczyński, B.; Kotarba, A.; Sojka, Z. Thermal stability and repartition of potassium promoter between the support and active phase in the $\text{K-Co}_{2.6}\text{Zn}_{0.4}\text{O}_4/\alpha\text{-Al}_2\text{O}_3$ catalyst for N_2O decomposition: Crucial role of activation temperature on catalytic performance. *Appl. Catal. B: Environ.* **2017**, *205*, 597–604. [[CrossRef](#)]

37. Ladgaonkar, B.P.; Vaingankar, A.S. X-ray diffraction investigation of cation distribution in $\text{Cd}_x\text{Cu}_{1-x}\text{Fe}_2\text{O}_4$ ferrite system. *Mater. Chem. Phys.* **1998**, *56*, 280–283. [[CrossRef](#)]
38. Raghuvanshi, S.; Mazaleyrat, F.; Kane, S.N. $\text{Mg}_{1-x}\text{Zn}_x\text{Fe}_2\text{O}_4$ nanoparticles: Interplay between cation distribution and magnetic properties. *AIP Adv.* **2018**, *8*, 047804. [[CrossRef](#)]
39. Sukandhiya, S. Effect of Mn^{2+} ions on Structural and Magnetic properties of Co-precipitated Ni-Cr nano ferrite for Potential applications as MRI Contrast agent. *Int. J. Res. Appl. Sci. Eng. Technol.* **2018**, *6*, 3713–3721. [[CrossRef](#)]
40. Wu, M.; Zhan, W.; Guo, Y.; Guo, Y.; Wang, Y.; Wang, L.; Lu, G. An effective Mn-Co mixed oxide catalyst for the solvent-free selective oxidation of cyclohexane with molecular oxygen. *Appl. Catal. A: Gen.* **2016**, *523*, 97–106. [[CrossRef](#)]
41. Trivedi, S.; Prasad, R. Reactive calcination route for synthesis of active Mn- Co_3O_4 spinel catalysts for abatement of CO- CH_4 emissions from CNG vehicles. *J. Environ. Chem. Eng.* **2016**, *4*, 1017–1028. [[CrossRef](#)]
42. Larimi, A.S.; Kazemeini, M.; Khorasheh, F. Highly selective doped Pt-MgO nano-sheets for renewable hydrogen production from APR of glycerol. *Int. J. Hydrog. Energy* **2016**, *41*, 17390–17398. [[CrossRef](#)]
43. Jung, D.H.; Umirov, N.; Kim, T.; Bakenov, Z.; Kim, J.S.; Kim, S.S. Thermal and Structural Stabilities of Li_xCoO_2 Cathode for Li Secondary Battery Studied by a Temperature Programmed Reduction. *Eurasian Chem.-Technol. J.* **2019**, *21*, 3–12. [[CrossRef](#)]
44. Pacultová, K.; Karásková, K.; Kovanda, F.; Jiráťová, K.; Šrámek, J.; Kustrowski, P.; Kotarba, A.; Chromčáková, Ž.; Kočí, K.; Obalová, L. K-doped Co-Mn-Al mixed oxide catalyst for N_2O abatement from nitric acid plant waste gases. Pilot plant studies. *Ind. Eng. Chem. Res.* **2016**, *55*, 7076–7084. [[CrossRef](#)]
45. Cheng, H.; Huang, Y.; Wang, A.; Li, L.; Wang, X.; Zhang, T. N_2O decomposition over K-promoted Co-Al catalysts prepared from hydrotalcite-like precursors. *Appl. Catal. B: Environ.* **2009**, *89*, 391–397. [[CrossRef](#)]
46. Imanaka, N.; Masui, T. Advances in direct NO_x decomposition catalysts. *Appl. Catal. A: Gen.* **2012**, *431*, 1–8. [[CrossRef](#)]
47. Smoláková, L.; Frolich, K.; Troppová, I.; Kutálek, P.; Kroft, E.; Čapek, L. Determination of basic sites in Mg-Al mixed oxides by combination of TPD- CO_2 and CO_2 adsorption calorimetry. *J. Therm. Anal. Calorim.* **2017**, *127*, 1921–1929. [[CrossRef](#)]
48. Hong, W.-J.; Iwamoto, S.; Inoue, M. Direct NO decomposition over a Ce-Mn mixed oxide modified with alkali and alkaline earth species and CO_2 -TPD behavior of the catalysts. *Catal. Today* **2011**, *164*, 489–494. [[CrossRef](#)]
49. Kotarba, A.; Hagstrom, M.; Engvall, K.; Pettersson, J.B.C. High pressure desorption of K^+ from iron ammonia catalyst migration of the promoter towards Fe active planes. *Catal. Lett.* **2004**, *95*, 93–97. [[CrossRef](#)]
50. Iwakuni, H.; Shinmyou, Y.; Yano, H.; Matsumoto, H.; Ishihara, T. Direct decomposition of NO into N_2 and O_2 on BaMnO_3 -based perovskite oxides. *Appl. Catal. B: Environ.* **2007**, *74*, 299–306. [[CrossRef](#)]
51. Goto, K.; Ishihara, T. Direct decomposition of NO into N_2 and O_2 over $\text{Ba}_3\text{Y}_{3.4}\text{Sc}_{0.6}\text{O}_9$. *Appl. Catal. A: Gen.* **2011**, *409*, 66–73. [[CrossRef](#)]
52. Tofan, C.; Klvana, D.; Kirchnerova, J. Decomposition of nitric oxide over perovskite oxide catalysts: Effect of CO_2 , H_2O and CH_4 . *Appl. Catal. B* **2002**, *36*, 311–323. [[CrossRef](#)]
53. Obalová, L.; Maniak, G.; Karásková, K.; Kovanda, F.; Kotarba, A. Electronic nature of potassium promotion effect in Co-Mn-Al mixed oxide on the catalytic decomposition of N_2O . *Catal. Commun.* **2011**, *12*, 1055–1058. [[CrossRef](#)]
54. Klyushina, A.; Pacultová, K.; Karásková, K.; Jiráťová, K.; Ritz, M.; Fridrichová, D.; Volodarskaja, A.; Obalová, L. Effect of preparation method on catalytic properties of Co-Mn-Al mixed oxides for N_2O decomposition. *J. Mol. Catal. A: Chem.* **2016**, *425*, 237–247. [[CrossRef](#)]

